The distribution and origin of smooth plains on Mercury

Brett W. Denevi,[1] Carolyn M. Ernst,[1] Heather M. Meyer,[1] Mark S. Robinson,[2] Scott L. Murchie,[1] Jennifer L. Whitten,[3] James W. Head,[3] Thomas R. Watters,[4] Sean C. Solomon,[5,6] Lillian R. Ostrach,[2] Clark R. Chapman,[7] Paul K. Byrne,[5] Christian Klimczak,[5] and Patrick N. Peplowski[1]

Received 31 October 2012; revised 26 March 2013; accepted 29 March 2013; published 6 May 2013.

[1] Orbital images from the MESSENGER spacecraft show that ~27% of Mercury's surface is covered by smooth plains, the majority (>65%) of which are interpreted to be volcanic in origin. Most smooth plains share the spectral characteristics of Mercury's northern smooth plains, suggesting they also share their magnesian alkali-basalt-like composition. A smaller fraction of smooth plains interpreted to be volcanic in nature have a lower reflectance and shallower spectral slope, suggesting more ultramafic compositions, an inference that implies high temperatures and high degrees of partial melting in magma source regions persisted through most of the duration of smooth plains formation. The knobby and hummocky plains surrounding the Caloris basin, known as Odin-type plains, occupy an additional 2% of Mercury's surface. The morphology of these plains and their color and stratigraphic relationships suggest that they formed as Caloris ejecta, although such an origin is in conflict with a straightforward interpretation of crater size–frequency distributions. If some fraction is volcanic, this added area would substantially increase the abundance of relatively young effusive deposits inferred to have more mafic compositions. Smooth plains are widespread on Mercury, but they are more heavily concentrated in the north and in the hemisphere surrounding Caloris. No simple relationship between plains distribution and crustal thickness or radioactive element distribution is observed. A likely volcanic origin for some older terrain on Mercury suggests that the uneven distribution of smooth plains may indicate differences in the emplacement age of large-scale volcanic deposits rather than differences in crustal formational process.

Citation: Denevi, B. W., et al. (2013), The distribution and origin of smooth plains on Mercury, *J. Geophys. Res. Planets*, *118*, 891–907, doi:10.1002/jgre.20075.

1. Introduction

[2] Large portions of Mercury's surface are covered by smooth plains having densities of impact craters consistent with ages younger than the cessation of the late heavy bombardment of the inner solar system [*Strom et al*., 1975, 2008; *Trask and Guest*, 1975; *Spudis and Guest*, 1988; *Denevi et al*., 2009; *Head et al*., 2011]. In Mariner 10 images of the hemisphere of Mercury from ~175°E to 345°E (from the eastern portion of the Caloris basin to just east of Kuiper crater), smooth plains were observed to display morphologies consistent with an origin by effusive volcanism (e.g., flooding and embayment relationships and lunar-mare-type contractional wrinkle ridges) [*Murray et al*., 1974; *Strom et al*., 1975; *Trask and Guest*, 1975; *Trask and Strom*, 1976; *Spudis and Guest*, 1988]. However, on the basis of the nearly concurrent finding from the Apollo 16 mission that lunar light plains originated as fluidized impact ejecta rather than volcanic flows [e.g., *Eggleton and Schaber*, 1972], an alternative hypothesis for the origin of smooth plains on Mercury was proposed [*Wilhelms*, 1976]. Many of the large plains units imaged by Mariner 10 surround the Caloris basin and lack clear albedo contrasts indicative of lunar-like compositional differences. No definitive volcanic landforms such as vents or domes were seen in Mariner 10 images, and no craters that are both younger than the Caloris basin and older than the plains within and around Caloris were found [*Wilhelms*, 1976]. On these grounds, it was suggested that at least some of the smooth plains on Mercury may have formed as fluidized ejecta

[1]The Johns Hopkins University Applied Physics Laboratory, Laurel, Maryland, USA.
[2]School of Earth and Space Exploration, Arizona State University, Tempe, Arizona, USA.
[3]Department of Geological Sciences, Brown University, Providence, Rhode Island, USA.
[4]Center for Earth and Planetary Studies, National Air and Space Museum, Smithsonian Institution, Washington, D.C., USA.
[5]Department of Terrestrial Magnetism, Carnegie Institution of Washington, Washington, D.C., USA.
[6]Lamont-Doherty Earth Observatory, Columbia University, Palisades, New York, USA.
[7]Southwest Research Institute, Boulder, Colorado, USA.

Corresponding author: B. W. Denevi, Space Department, The Johns Hopkins University Applied Physics Laboratory, 11100 Johns Hopkins Road, Laurel, MD 20723, USA. (Brett.Denevi@jhuapl.edu)

2169-9097/13/10.1002/jgre.20075

deposits from one or more basin-forming impact events in a similar manner to the Cayley plains visited by Apollo 16 [*Wilhelms*, 1976].

[3] Mariner 10 images acquired through two color filters (355 and 575 nm) initially showed an apparent lack of correlation between color units and geologic units [*Hapke et al*., 1980; *Rava and Hapke*, 1987]. When these images were reprocessed with an improved calibration, however, the smooth plains near Rudaki crater were found to display a more steeply sloped spectral reflectance at near-ultraviolet to visible wavelengths, a characteristic interpreted to result from a lower abundance of an opaque mineral component [*Robinson and Lucey*, 1997]. This correlation of spectral contrast with morphology is evidence for a compositional difference between plains and their surroundings, as would be expected for volcanic emplacement. Recalibrated Mariner 10 clear filter data also show that some plains units, such as Borealis Planitia, have a higher albedo than average for Mercury [*Denevi and Robinson*, 2008].

[4] Data from the MErcury Surface, Space ENvironment, GEochemistry, and Ranging (MESSENGER) spacecraft provide the evidence required to better discriminate the origin of plains units. Volcanic landforms, including a small shield volcano and other volcanic vents, have been identified within the Caloris basin and across the planet, and plains units have been observed far from any large basins [*Head et al*., 2008, 2009a, 2009b, 2011; *Murchie et al*., 2008; *Gillis-Davis et al*., 2009; *Kerber et al*., 2009, 2011; *Goudge et al*., 2012]. Color relationships also support a volcanic origin. Plains units often exhibit contrasts in color from their surroundings and have a range of spectral properties, from the high-reflectance red plains (HRP) to low-reflectance blue plains (LBP) [*Robinson et al*., 2008; *Denevi et al*., 2009], where "red" and "blue" denote spectral slopes respectively greater and less than average. The compositional differences suggested by these color contrasts were confirmed with measurements from MESSENGER's X-Ray Spectrometer (XRS). HRP-type areas correspond to a low-Fe (no more than 4 wt% Fe) basalt-like composition, and regions with lower reflectance are also low in Fe but have higher Mg/Si and Ca/Si and lower Al/Si and are interpreted to have a more ultramafic composition [*Nittler et al*., 2011; *Weider et al*., 2012].

[5] Despite resolution of the volcanic origin of many plains units, there remain terrains for which no definitive evidence on origin has yet been found. The plains that surround the Caloris basin in particular continue to challenge simple interpretations. The crater population of these plains suggests that they are younger than both the Caloris interior plains and the basin itself [*Murray et al*., 1975; *Strom et al*., 2008; *Fassett et al*., 2009]. If so, this age relation leaves volcanism as the only plausible mechanism for the formation of such relatively young, widespread deposits. However, lunar studies indicate that there can be an ambiguity in the ages of plains inferred to be related to major basin-forming events. Some lunar light plains are estimated on the basis of crater characteristics to be younger than the basins with which they are spatially associated [*Boyce et al*., 1974] or younger than all large basins [*Neukum*, 1977], perhaps calling into question a straightforward interpretation of the cratering histories of these regions or suggesting an alternative origin for some light plains [*Neukum*, 1977]. The hummocky textures and kilometer-scale knobs found in some portions of the circum-Caloris plains (Odin Formation) were interpreted to have formed as ejecta from the Caloris impact event, consistent with an impact origin for these plains [*Trask and Guest*, 1975; *McCauley et al*., 1981; *Guest and Greeley*, 1983]. However, in some regions, the blocks may also have been embayed and partially buried by later volcanic resurfacing [*Fassett et al*., 2009]. The color properties in this region and the variegated and diffuse boundaries of units also provide no clear evidence for volcanism [*Denevi et al*., 2009].

Table 1. Crater Size–Frequency Distributions for Selected Plains Units on Mercury[a]

Region	Central Latitude	Central Longitude	Area (km^2)	$N(10)$	$N(20)$
Rudaki plains	3°S	305°E	9.8×10^4	51 ± 23	10 ± 10
South of Rachmaninoff	6°N	70°E	3.6×10^5	58 ± 13	17 ± 7
East of Caloris	28°N	194°E	2.1×10^5	56 ± 16	19 ± 9
West of Caloris	19°N	135°E	4.1×10^5	91 ± 15	25 ± 8
Caloris interior	31°N	163°E	1.7×10^6	80 ± 7	26 ± 4
South of Caloris	9°S	169°E	3.7×10^5	92 ± 16	32 ± 9
Beethoven	19°S	236°E	2.2×10^5	82 ± 19	32 ± 12
Rembrandt	33°S	87°E	2.9×10^5	103 ± 19	45 ± 12
Intercrater plains	16°N	23°E	1.0×10^6	217 ± 14	94 ± 9

[a] $N(10)$ and $N(20)$ values give the cumulative number of craters per million square kilometers larger than 10 km or 20 km in diameter, respectively.

[6] On the basis of Mariner 10 and MESSENGER flyby images, smooth plains were estimated to cover 15–40% of Mercury's surface [*Strom et al*., 1975; *Spudis and Guest*, 1988; *Denevi et al*., 2009]. Although flyby images combined to cover ~98% of the planet, some regions were seen at illumination and viewing conditions that were not well suited for observing morphology (i.e., large emission angles and small solar incidence angles, both measured from the surface normal, or pixel scales >1 km) and so were not mapped [*Denevi et al*., 2009].

[7] Images acquired during MESSENGER's orbital operations now provide the means to assess the spatial and temporal distribution of plains units across Mercury in a globally consistent manner. From imaging coverage acquired at optimized geometries and near-complete topographic data, we created a global map of the distribution of smooth plains and constrained the range of their ages. From compositional information obtained with multiple instruments, we examine here the range of compositions of smooth plains units and we assess possible variations in composition through time. The goal of this work is to evaluate the history of plains formation on Mercury recorded in these younger units, with implications for older plains units, the history of which has been partially clouded by the effects of the late heavy bombardment. What processes have worked to create the surface of Mercury that we see today?

2. Data and Methods

[8] As the basis for mapping the distribution of smooth plains units on Mercury, we used images from MESSENGER's Mercury Dual Imaging System (MDIS), which includes a narrow-angle camera (NAC; 1.5° field of view) and a wide-angle camera (WAC; 10.5° field of view) [*Hawkins et al*., 2007]. Surface morphology was analyzed using images from the monochrome base map campaign, which covers more

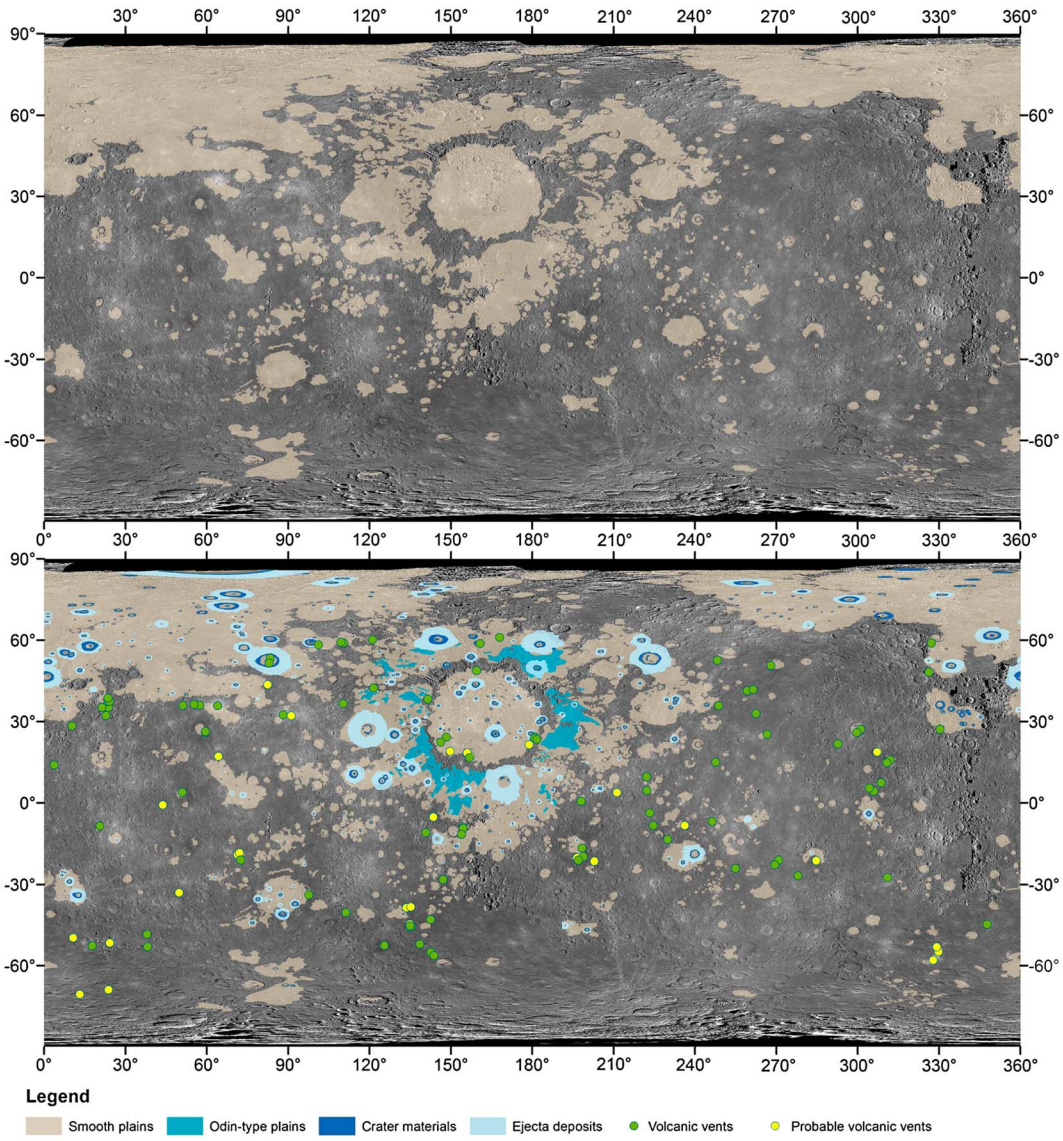

Figure 1. (top) Map of smooth plains (tan) on Mercury as defined in this study. As closely as possible, the original extent of smooth plains was mapped, regardless of later modification by impact craters. (bottom) Smooth plains along with the approximate boundaries of Odin-type plains (turquoise). Superposed craters >20 km in diameter along with crater materials (rims, terraces, peaks) are shown in navy blue and ejecta deposits in light blue. Also shown are locations of irregular, rimless depressions interpreted to be volcanic vents (green circles) or "probable" volcanic vents (yellow circles), for which our identification of a vent-like feature was more tentative. The maps are in a simple cylindrical projection; the central longitude is 180°E.

than 99% of the planet. During its primary orbital mission, MESSENGER was in a highly eccentric orbit, with an apoapsis altitude of over 15,000 km in the southern hemisphere and periapsis altitude in the north as low as 200 km. The monochrome base map includes 25 μrad/pixel NAC images (largely in the southern hemisphere) and 178 μrad/pixel WAC 750 nm filter images (mainly in the northern hemisphere) acquired at low emission angles and solar incidence angles targeted to be near 68° so as to highlight morphology. The combination of NAC and WAC images and selective on-chip binning results in an average pixel scale of 220 m (resampled here to 250 m/pixel). Average solar incidence and emission angles are 69° and 11°, respectively. At the time of this writing, MDIS is acquiring a second monochrome base map with a larger average incidence angle (80°), and these images were also consulted where available. We supplemented the monochrome base maps with WAC color image sequences (either three or eight filters between 430 and 1020 nm) acquired near nadir at small solar incidence angles and with targeted NAC images at pixel scales as small as 10 m. Topographic information from the Mercury Laser Altimeter [*Zuber et al.*, 2012] and stereo imaging [*Oberst et al.*, 2010; *Preusker et al.*, 2011, 2012; *Gaskell et al.*, 2011; *Becker et al.*, 2012] was used to compare relative elevations of terrain.

[9] We mapped the distribution of young plains on Mercury at a scale of 1:1.25 M, following unit definitions established by *Trask and Guest* [1975] from Mariner 10

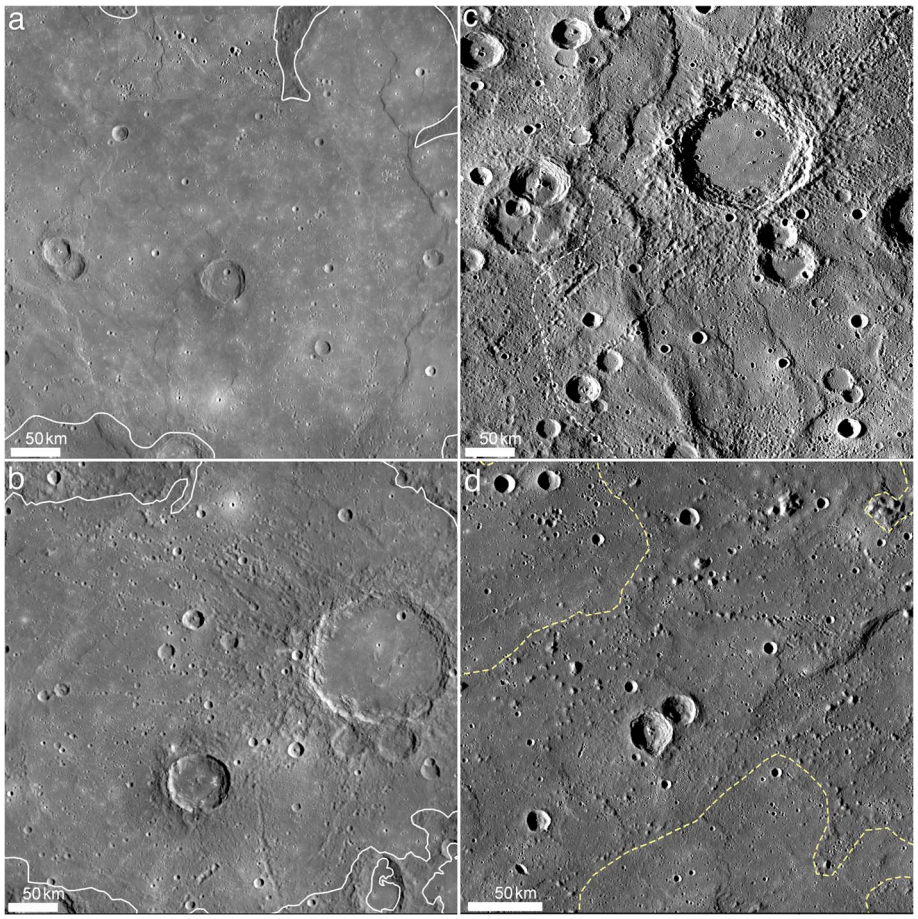

Figure 2. The range of plains morphologies included in our map, each in an equirectangular projection centered on the indicated latitude and longitude. (a) An example of some of the youngest smooth plains south of Rachmaninoff basin (5°N, 75°E). (b) Smooth plains within Beethoven basin (20°S, 245°E) that are more heavily cratered than those in Figure 2a. These plains were originally mapped from Mariner 10 images as intermediate plains [*King and Scott*, 1990] (see Figure 3). (c) Dashed white lines indicate the approximate boundary of the most heavily cratered plains that we still consider to be smooth (35°N, 330°E). The incidence angles for images in this region of the monochrome mosaic are >80°, making it more difficult to compare directly regions seen at more typical incidence angles (average 69°). (d) Dashed yellow lines indicate the approximate boundary between knobby Odin-type plains (center of image) and smooth plains found to the southwest of the Caloris basin (20°N, 140°E). The Odin plains often display gradational boundaries with the surrounding smooth plains, and nearby smooth plains often contain isolated knobs. The edge of Caloris rim materials is seen in the northeast corner of this image, and in many places no clear embayment relationships are observed between the circum-Caloris plains and the Caloris rim.

images. Smooth plains were defined as relatively sparsely cratered, essentially level terrains that typically have distinct boundaries with adjacent terrain [*Trask and Guest*, 1975]. Topographic information derived from stereo images and laser altimetry confirm the plains to be level over short distances, but broad areas within Caloris and the northern plains have substantial long-wavelength topographic variations suggestive of post-emplacement deformation [*Oberst et al*., 2010; *Zuber et al*., 2012], a finding that warrants some modification to this definition. Thus, we define smooth plains as smooth, relatively sparsely cratered terrain that displays sharp boundaries with adjacent regions and is level to gently sloped over a baseline of ~100–200 km. *Trask and Guest* [1975] noted that an abundance of tectonic landforms, including wrinkle ridges and scarps, often gives smooth plains a gently rolling appearance, which is also consistent with observations from MESSENGER data.

[10] Smooth plains are distinguished from older intercrater plains, which are defined as level to gently rolling terrain with an abundant population of secondary craters 5–10 km in diameter, more gradational boundaries, and typical locations between and around large craters [*Trask and Guest*, 1975]. Later Mariner 10 quadrangle maps also included an "intermediate plains" unit, with characteristics similar to those of the smooth plains but with slightly more superposed craters and more gradational boundaries [e.g., *Trask and Dzurisin*, 1984]. On the basis of the *Trask and Guest* [1975] definitions, however, intermediate plains would be considered smooth plains, but substantial differences exist between individual plains exposures [*Whitten et al*., 2012].

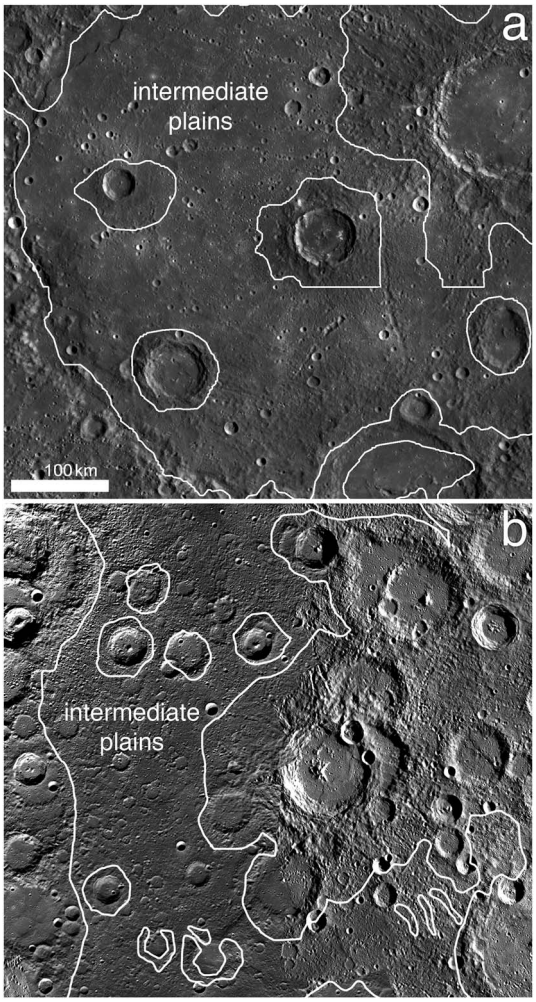

Figure 3. Intermediate plains as mapped from Mariner 10 images [*Grolier and Boyce*, 1984; *Spudis and Prosser*, 1984; *King and Scott*, 1990]. (a) Plains within Beethoven basin (20°S, 245°E) mapped as intermediate plains have been included as smooth plains in this paper (see Figure 2b). Several straight edges indicate boundaries between separate quadrangle maps. (b) An example of intermediate plains (75°N, 210°E) near Jokai crater that was not included in our map of smooth plains. The region has a rougher surface and lacks clear boundaries. Scale same as shown in (a).

We assess the utility of dividing young plains into smooth versus intermediate plains in section 3.1.

[11] In this study, we excluded isolated smooth plains units (far from any other smooth plains deposits) that are contained within a single impact crater and are smaller than ~100 km across (i.e., those most likely to have formed from impact melt). As closely as possible, we mapped the original extents of smooth plains, regardless of later modification of boundaries by impact craters (primary and secondary). In some places, such mapping required estimation of where the margin would be if not for the presence of a large impact crater, or the assumption that smooth plains were contiguous before formation of an impact crater. We then mapped superposed craters larger than 20 km in diameter as "crater materials" (rims, terraces, central peaks, or peak rings), as well as their ejecta deposits where such material substantially altered the appearance of the plains. In this way, we assessed both the original extent of smooth plains and their present-day exposures. Given the uncertain origin of knobby, Odin-type plains, we separately mapped their extent within the circum-Caloris plains. However, as their boundaries are in places gradational between smooth and knobby plains, some isolated knobs are included in regions mapped as smooth plains surrounding Caloris.

[12] In addition to considering the morphology and qualitatively assessing the relative crater densities of plains units, we measured the size–frequency distributions of impact craters on key plains occurrences. We selected nine representative regions (Table 1) ranging in size from 9.8×10^4 to 1.7×10^6 km^2 and, from the monochrome base map, recorded the sizes and locations of superposed craters larger than 2 km in diameter, making an effort to avoid those craters in chains or clusters most likely to be secondary in origin. The interior plains of Caloris were included to facilitate comparisons between our counts and those of previous workers [*Strom et al*., 2008; *Fassett et al*., 2009].

[13] Finally, to aid in interpreting the origin of smooth plains units, we mapped the distribution of volcanic vents. Candidate vents are all irregular, rimless depressions identifiable in the monochrome base map. As all such features were identified primarily from this mosaic, no observational bias due to MESSENGER's eccentric orbit affects this data set. Many but not all of these depressions are surrounded by distinctly colored (higher reflectance and steeper spectral slope) halos identifiable in the WAC color base map. If a clear origin could not be determined from base map imagery alone, targeted NAC images (if available) were analyzed or the feature was categorized as a "probable" volcanic vent. The landforms mapped included those identified previously as the sources of pyroclastic deposits [*Kerber et al*., 2009, 2011; *Goudge et al*., 2012] and irregular depressions that may have formed through collapse after the subsurface withdrawal of magma from a magma chamber [*Gillis-Davis et al*., 2009]. The features are distinguished from "hollows" (irregular depressions thought to form from loss of a volatile material) by their larger size and lack of shallow (blue) spectral slope [*Blewett et al*., 2011; *Goudge et al*., 2012].

3. Results

3.1. Mapped Smooth Plains

[14] The distribution of smooth plains is shown in Figure 1. Smooth plains, when mapped as closely to their original extent as possible, cover 27% of the planet. An additional 2% of the surface is mapped as Odin-type plains with kilometer-scale knobs. Although we have excluded isolated smooth plains units contained entirely within craters <100 km in diameter, and it is likely that we have missed small occurrences of smooth plains for which classification is debatable, the exclusion of such areas would not substantially change our results. The range in appearance of plains included in our map is shown in Figure 2, from plains with sharp contacts and the lowest crater densities (e.g., Figure 2a) through regions with sharp contacts but more superposed craters (e.g., Figure 2b), to the most cratered regions we still mapped as smooth plains (Figure 2c). The area shown in Figure 2c is also an example of a region for which inclusion

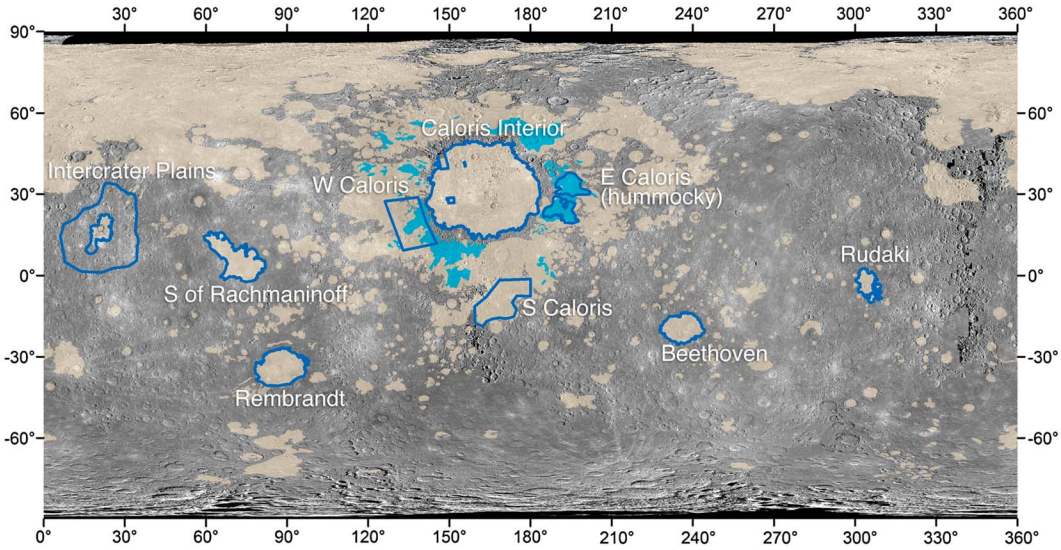

Figure 4. Locations of count areas for crater size–frequency distributions shown in Figures 5, 6, and 7 and listed in Table 1.

in our map was potentially ambiguous. Whereas the area is relatively heavily cratered, there are still large portions where modification by secondary cratering has been minor and the boundaries with surrounding terrain are clear. This area of the monochrome mosaic was imaged at larger than average incidence angles (>80°), resulting in the appearance of a rougher surface (as even small topographic features cast long shadows), making a comparison with other smooth plains imaged at moderate incidence angles difficult. Finally, an example of Odin-type hummocky plains is shown in Figure 2d. The boundaries of these plains are often gradational, and their distribution shown in Figure 1 is approximate.

[15] In comparing our mapped plains in regions of imaging overlap with Mariner 10, we find that the distribution of smooth plains is generally similar to that shown in earlier maps. Some differences exist for regions mapped as intermediate plains on the basis of Mariner 10 data. We compared our results with large regions of intermediate plains on the Mariner 10 quadrangle maps, including the plains within Beethoven basin and those near Jokai crater [*Grolier and Boyce*, 1984; *Spudis and Prosser*, 1984; *King and Scott*, 1990] (Figure 3). By the classification of *Trask and Guest* [1975], the Beethoven plains (Figure 3a) were included in our map as smooth plains, whereas the plains near Jokai were not included and may be better classified as intercrater

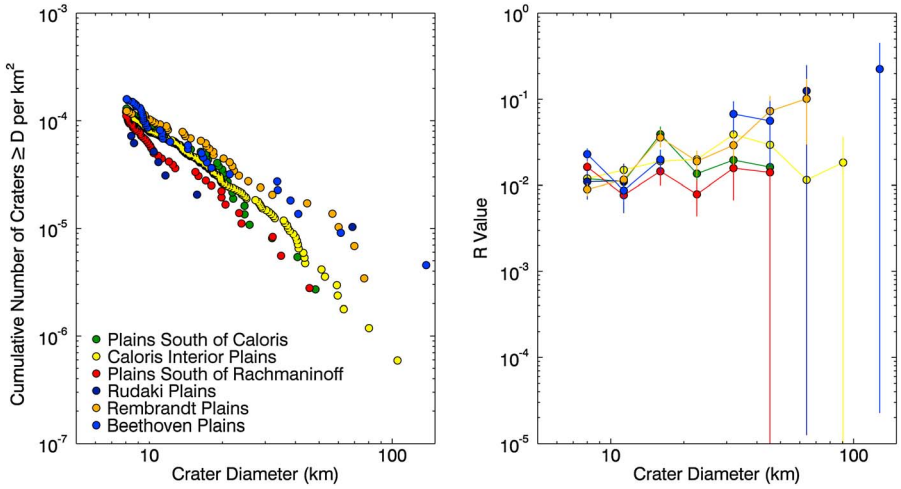

Figure 5. Crater size–frequency distributions for the range of smooth plains areas in Figure 4 show a relatively narrow range of crater densities. Here and in subsequent figures, an unbinned cumulative histogram is shown on the left, and on the right is an R plot with root-two binning; errors shown equal the square root of the number of craters in a given bin [*Crater Analysis Techniques Working Group*, 1979]. The crater size–frequency distributions of the smooth plains are most similar in shape to the characteristic "Population 2" [*Strom et al.*, 2005] of surfaces formed largely after the cessation of the late heavy bombardment.

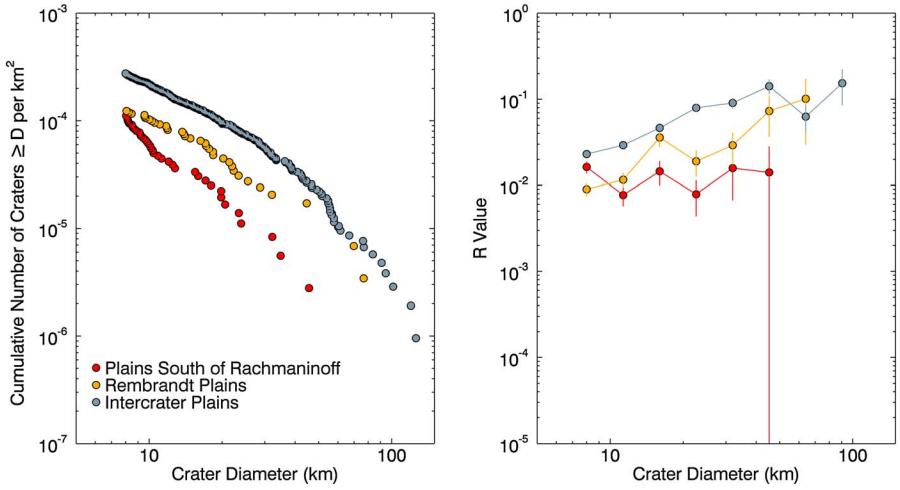

Figure 6. Crater size–frequency distribution for the most sparsely and most heavily cratered smooth plains units (Table 1) are displayed for comparison with a region of intercrater plains (location shown in Figure 4). A separation in cratering populations is seen between smooth plains and intercrater plains, with the intercrater plains more closely following the "Population 1" shape of surfaces affected by the late heavy bombardment [*Strom et al*., 2005].

plains, as they have a host of secondary craters and poorly defined boundaries. We note that the variation in illumination and viewing conditions in Mariner 10 images is likely to have contributed to the large range of surface roughnesses in areas previously mapped as intermediate plains (the Beethoven plains, in particular, were imaged when near the subsolar point). Future mapping of these older regions may permit intermediate and intercrater plains to be distinguished, but for the work here and the recent study by *Whitten et al*. [2012], the definitions of smooth and intercrater plains are sufficient to describe the range of morphologies observed.

3.2. Density of Impact Craters on the Plains

[16] As the definitions of plains are based in part on the density of superposed impact craters, we examined whether a quantitative assessment of crater size–frequency distributions could aid more qualitative visual measures for discriminating smooth plains. For the representative smooth plains regions (Table 1, Figure 4), there is a relatively narrow range of variation in cratering history (Figure 5). The cumulative number of craters larger than 20 km in diameter per million square kilometers, $N(20)$, provides a metric for comparing the crater populations among smooth plains. The youngest large exposures, a broad expanse of plains to the south of Rachmaninoff basin and the plains near Rudaki crater, have $N(20)$ values in the range 10–17. The oldest large exposure of smooth plains, that within Rembrandt basin, has an $N(20)$ value of 45 ± 12. When the cumulative size–frequency distributions are normalized to a power law slope of -3 on a standard R plot [*Crater Analysis Techniques Working Group*, 1979] (Figure 5b), all of the representative smooth plains units have the characteristic "Population 2" shape indicative of an impactor population that largely postdated late heavy bombardment [*Strom et al*., 2005]. In comparison, the representative intercrater plains unit has an $N(20)$ value of 94 ± 9, twice that of the most cratered smooth plains. Its R plot indicates cratering by "Population 1" impactors during the late heavy bombardment, as found for more heavily cratered terrain on Mercury (Figure 6) [*Strom et al*., 2008, 2011; *Fassett et al*., 2011; *Ostrach et al*., 2011]. Thus, we find a clear distinction in crater density between smooth and intercrater plains. If volcanic in origin, this population of smooth plains is analogous to the extant lunar maria, emplaced largely after the cessation of the late heavy bombardment.

[17] The circum-Caloris plains display a range of morphologies from smooth to knobby. Whereas smooth plains are defined as having sharp boundaries with surrounding terrain, such a characteristic does not always apply to the plains surrounding Caloris. Knobby, Odin-type plains are observed to grade to smooth plains in places, with an associated decrease in the density of knobs. This gradational relationship may be because volcanic smooth plains have embayed the knobs, burying them to varying degrees, or because the smooth plains in this region share an origin with the knobs as Caloris ejecta. To help discriminate between these two scenarios, we selected three representative areas for comparison of their crater populations (smooth, moderately knobby, and knobby). These regions also show variations in their style and degree of tectonic deformation. The first region, to the south of the basin, is an extension of Tir Planitia and shares the typical characteristics of smooth plains (Figure 7f) with sharp boundaries and only rare positive relief features that could represent Odin-type knobs. The area displays color contrasts with some surrounding terrain, and the presence of wrinkle ridges attests to contractional deformation within these plains. The second study area is in the plains to the west of Caloris, which, although generally smooth, have more common exposures of knobs (Figure 7e). In contrast to the first region, there is a dearth of wrinkle ridges and tectonic deformation has instead been accommodated by lobate scarps [*Watters et al*., 2009b] that are in many cases radial to the basin. Any contact between these plains and the more typical smooth plains of the first region to the southeast is obscured by the 240-km-diameter Mozart basin (Figure 7). The third region, to the east of Caloris, is in the hummocky Odin plains (Figure 7d), with the highest

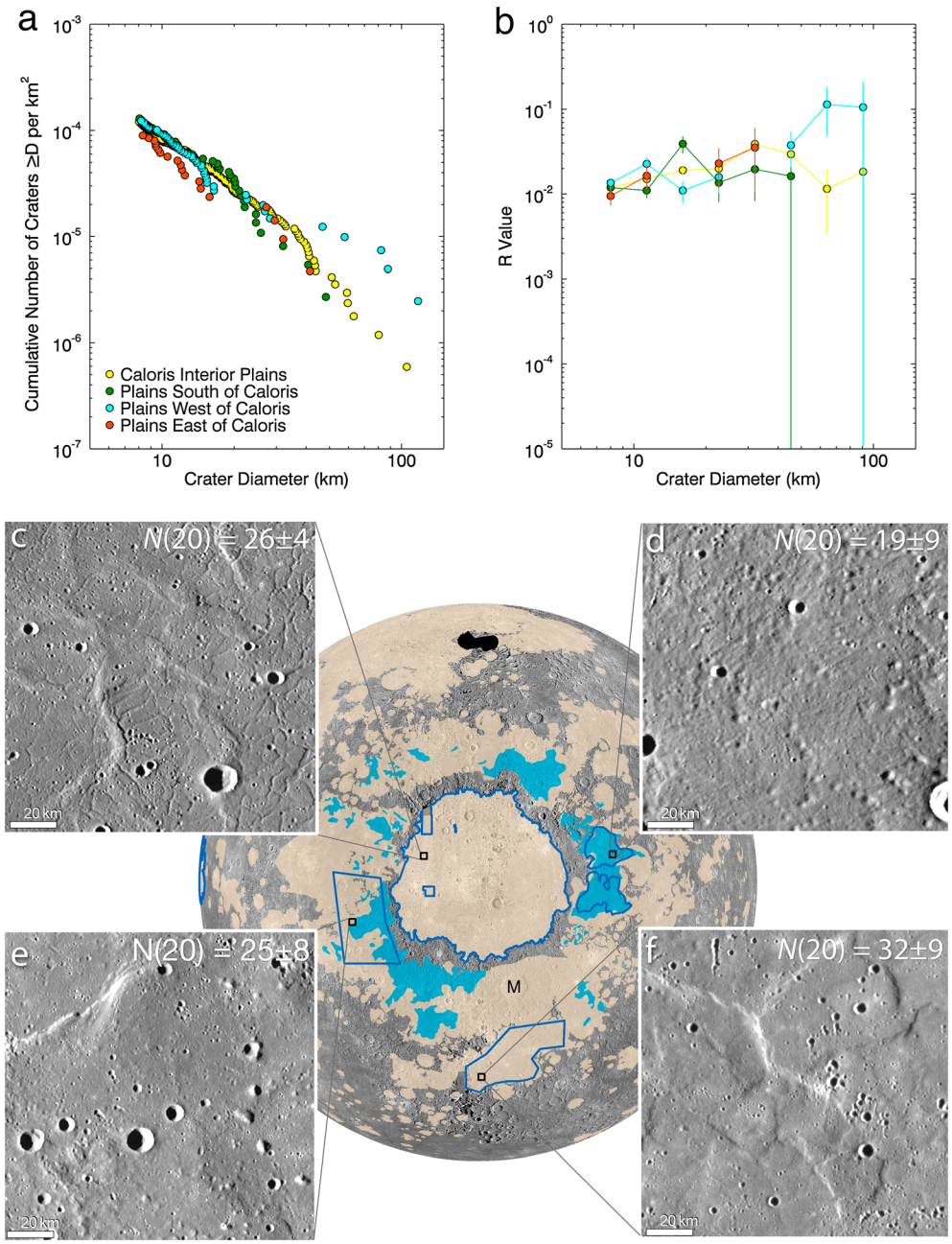

Figure 7. (a, b) The range of crater size–frequency distributions for plains associated with the Caloris basin; the locations of each count area are given in Table 1 and shown in navy blue in the map at bottom center. (c) Smooth plains within Caloris basin having a high concentration of wrinkle ridges and graben. (d) Hummocky plains to the east of Caloris. (e) A mixture of smooth plains with more isolated knobs to the west of Caloris. (f) Smooth plains to the south of Caloris with a high concentration of wrinkle ridges. Any contact between the plains deposits shown in Figures 7e and 7f is obscured by the Mozart basin, indicated with an "M" on the context image.

density of knobs among the three areas and a distinctly rougher texture. Contractional deformation here was also primarily accommodated by lobate scarps.

[18] The plains to the east and west of Caloris have a similar to slightly lower density of craters than the interior plains of Caloris, consistent with previous results [*Murray et al.*, 1974; *Strom et al.*, 2008; *Fassett et al.*, 2009] (Figures 7a and 7b, Table 1). The $N(20)$ value of the interior plains is 26 ± 4 (in agreement with the value of 23 ± 4 found by *Fassett et al.* [2009]), compared with 25 ± 8 for the smooth plains with a moderate density of knobs west of Caloris, and 19 ± 9 for the knobby Odin plains east of Caloris. The smooth plains to the south of Caloris have a slightly higher crater density, with $N(20) = 32 \pm 9$, than those of the interior. Interestingly, despite having been mapped as Caloris ejecta [*Trask and Guest*, 1975; *McCauley et al.*, 1981; *Guest and Greeley*, 1983] and displaying stratigraphic relationships that suggest embayment by

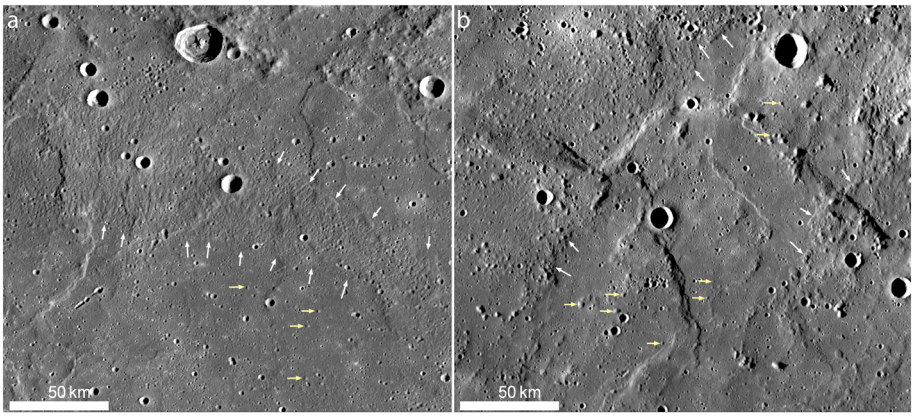

Figure 8. Examples of the relationship between smooth and hummocky plains outside of the Caloris basin. (a) A region to the east of Caloris (30°N, 200°E) where smooth plains appear to embay hummocky plains (white arrows indicate contact). Within the smooth plains, isolated knobs (yellow arrows) may be kipukas of a buried hummocky unit. (b) Similar relationships are observed to the southwest of Caloris (5°N, 147°E), with relatively sharp contacts between smooth and hummocky regions (white arrows) and isolated knobs or small clusters of knobs within the smooth plains (yellow arrows).

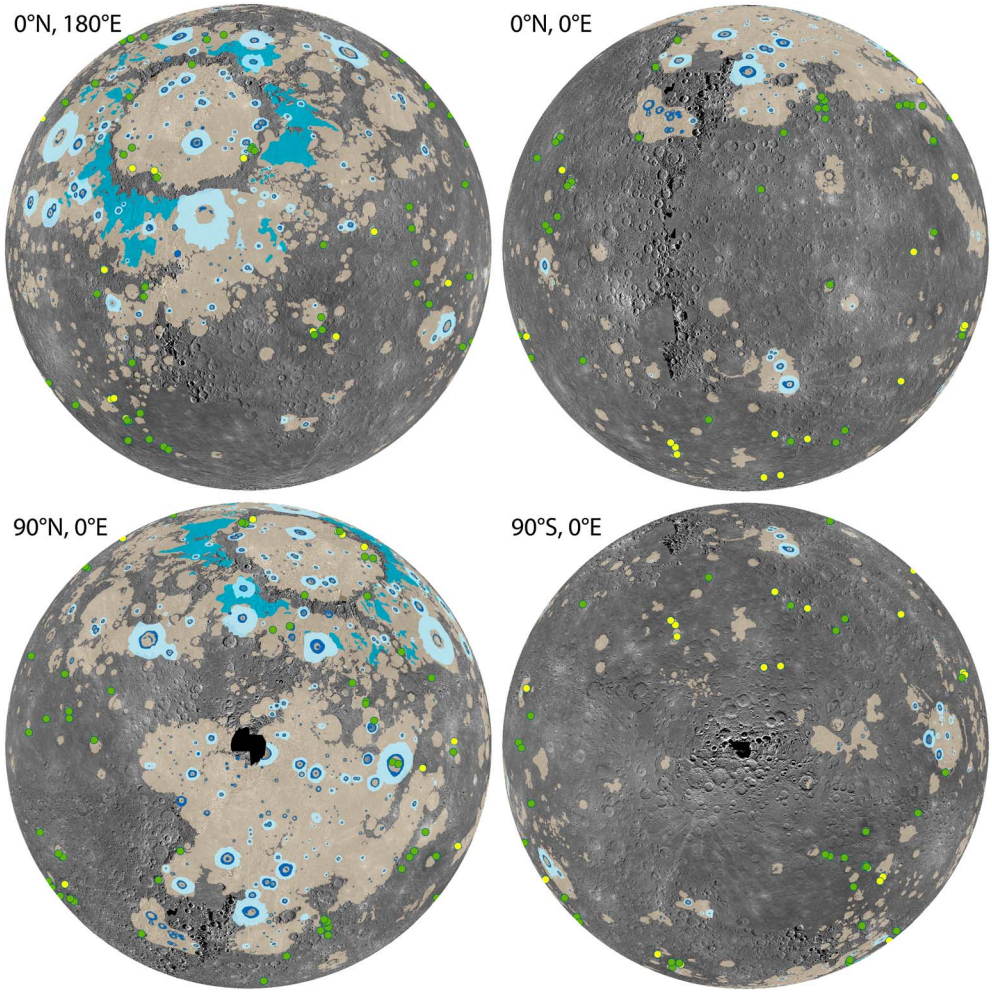

Figure 9. Four orthographic projections of the map shown in Figure 1b (labels give the central latitude and longitude of each projection). These views highlight the hemispherical differences in the areal abundances and distributions of smooth plains. Colors and symbols are the same as those shown in Figure 1b.

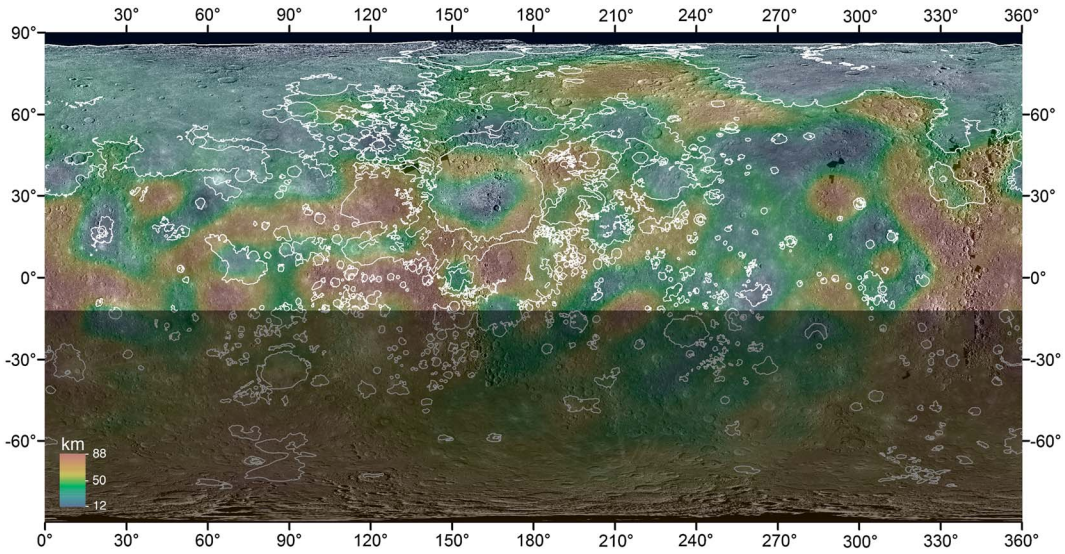

Figure 10. A comparison of the distribution of smooth plains (white outlines) to model crustal thickness values [*Smith et al*., 2012]. Some regions of smooth plains, including the northern plains and Sobkou Planitia, are found in regions of low crustal thickness, whereas considerable variation is seen in other regions, including the plains associated with Caloris. The shading in the south indicates where crustal thickness is unconstrained because of the lack of altimetry data as a result of MESSENGER's highly eccentric orbit and northern periapsis.

smooth plains (Figure 8), the knobby Odin plains have the lowest crater density of all plains associated with Caloris and the largest difference from the crater population of the Caloris rim materials, for which *Fassett et al*. [2009] found an $N(20)$ value of 54 ± 12. Although the crater populations of the circum-Caloris plains are substantially lower in density than for the Caloris rim materials, we find no clear stratigraphic relationships between the circum-Caloris plains and the rim of the basin; the units appear to grade smoothly from one to the next.

3.3. The Asymmetric Distribution of Smooth Plains

[19] As previously observed [*Denevi et al*., 2009], smooth plains are found across all longitudes and at nearly all latitudes. However, there is an asymmetry in the distribution of the most areally extensive occurrences. The majority of smooth plains are contained within three formations: the Caloris interior plains, described by *Murchie et al*. [2008] and *Watters et al*. [2009b]; the circum-Caloris plains; and the northern plains, described by *Head et al*. [2011]. These three areas together account for over half of the area of mapped plains and contribute to a large difference in plains concentrations between northern and southern hemispheres (Figure 9). Previous maps of smooth plains from only Mariner 10 images [*Spudis and Guest*, 1988] or from a combination of Mariner 10 and MESSENGER flyby images [*Denevi et al*., 2009] did not display as clearly the asymmetry in smooth plains distribution, and plains were earlier estimated to cover up to 40% of the surface. The difference in estimated fractional area is due to two main factors. First, a broad region centered on 0°E has a dearth of smooth plains. The majority of this area was not viewed by Mariner 10 and was imaged only at low solar incidence angles (near noon) and high emission angles (oblique viewing geometry) by MESSENGER during its Mercury flybys and was therefore not previously mapped. Second, orbital images show that previous work included some plains that are more heavily cratered than smooth plains and so are more appropriately classified as intercrater plains.

[20] The rimless, irregular depressions in our map interpreted to be volcanic vents [*Gillis-Davis et al*., 2009; *Kerber et al*., 2009, 2011; *Goudge et al*., 2012] are found almost entirely outside smooth plains, with some concentrated along the margins of large smooth plains deposits, consistent with the findings of *Head et al*. [2011], or within craters in isolated smooth plains exposures (Figure 1b). This distribution is consistent with smooth plains having formed largely by the emplacement of relatively low-viscosity flood basalts, which buried vents that may have once existed within their boundaries. Vents located outside large smooth plains deposits were preserved. However, we note that few vents are observed at high southern latitudes or at midlatitudes near 0°E, where there is also a lack of large-scale smooth plains deposits.

[21] Finally, we compared our map of smooth plains with that of crustal thickness [*Smith et al*., 2012] for the northern hemisphere of Mercury (Figure 10). Considerable variation in crustal thickness is found for regions of smooth plains. Some large deposits such as the northern plains and Sobkou Planitia are underlain by relatively thin crust. Other large deposits, especially those within and around the Caloris basin, have a large variation in crustal thickness. Additionally, there are regions of relatively low crustal thickness with no associated smooth plains, most conspicuously east of Sobkou near 50°N, 270°E.

4. Discussion

4.1. Plains Composition and Origin

[22] Morphologies and color properties revealed in images obtained from MESSENGER's flybys of Mercury and

subsequent orbital observations support a volcanic origin for the Caloris interior plains and northern plains [*Head et al*., 2008, 2011; *Murchie et al*., 2008; *Robinson et al*., 2008]. Other smooth plains deposits with clear embayment relations and color properties distinct from underlying terrain also provide strong evidence for an origin via effusive volcanism [e.g., *Head et al*., 2009a]. The majority of smooth plains occurrences are relatively high in reflectance, have steep spectral slopes, and have been classified as HRP [*Denevi et al*., 2009]. Thus far, the most detailed compositional information for HRP is for the northern plains, which have Mg/Si, Ca/Si, and Al/Si values that are consistent with a magnesian basalt-like lithology [*Nittler et al*., 2011; *Stockstill-Cahill et al*., 2012; *Weider et al*., 2012] with a relatively high abundance of K [*Peplowski et al*., 2012]. Analysis of XRS data also shows that the Caloris interior plains have a composition similar to that of the northern plains [*Weider et al*., 2012] except for a lower K abundance, perhaps due to higher maximum surface temperatures at Caloris that mobilize and redistribute this moderately volatile element from the Caloris plains [*Peplowski et al*., 2012]. By extension, the majority of smooth plains may share a magnesian alkali basalt composition, as they share HRP spectral properties. However, the lack of diagnostic absorption bands in reflectance spectra means that more work is required to confirm this suggestion. Plains of intermediate reflectance and spectral slope, such as those near Rudaki crater, may be compositionally related to the HRP via partial melting. Future analysis of XRS spectra from areas dominated by smooth plains of intermediate reflectance and further petrographic experiments such as those of *Charlier et al*. [2013] will help to elucidate the relationships among smooth plains compositions.

[23] But what of the circum-Caloris plains? Determining their origin has implications both for the distribution of volcanism on Mercury and for the evolution of lava compositions over time. The LBP spectral characteristics (low reflectance and shallower spectral slope) of these plains [*Robinson et al*., 2008; *Denevi et al*., 2009] are comparable in color to more heavily cratered terrain that predates the smooth plains and has been identified as having more mafic compositions than the northern plains [*Nittler et al*., 2011; *Weider et al*., 2012]. Direct observations of a portion of the western plains exterior to Caloris also show that they may be more ultramafic than other smooth plains [*Weider et al*., 2012]. If these plains are volcanic, their composition suggests that the thermal history of Mercury was such that the high source region temperatures required to achieve high degrees of partial melting of the planet's mantle (resulting in the generation of melts of more ultramafic composition) were not limited to Mercury's most ancient terrain but continued throughout much of the duration of smooth plains formation.

[24] Of the circum-Caloris plains, the smooth plains to the south and east of Caloris that make up Tir and Budh planitiae display the strongest evidence for volcanism. Those plains contain few knobs or other features thought to be associated with Caloris ejecta. They also contain a high density of wrinkle ridges [*Watters et al*., 2009a] and several wrinkle-ridge rings indicative of buried impact craters [*Klimczak et al*., 2012]. Although not diagnostic of volcanic plains, wrinkle ridges are typically associated with such deposits [e.g., *Watters*, 1988].

[25] However, for regions mapped as Odin-type knobby plains, the morphologic and stratigraphic relationships are more consistent with emplacement as Caloris impact ejecta, perhaps in combination with effusive and/or impact melt deposits. The knobby and hummocky textures observed within these plains are similar to those of plains associated with some lunar basins and interpreted to be impact ejecta (Figure 11) [e.g., *Wilhelms*, 1987]. Their morphology and spatial distribution led to the interpretation that the Odin plains observed by Mariner 10 were emplaced as ejecta from the Caloris impact event [*Murray et al*., 1974; *Strom et al*., 1975; *Trask and Guest*, 1975]. The knobby plains to the southwest and west of Caloris also lack the dense population of wrinkle ridges seen to the southeast [*Watters et al*., 2009b]. In many regions, the Odin-type plains appear to grade continuously into Caloris rim deposits (Figure 12). Several locations also show evidence of flow from the lower-reflectance Odin-type deposits into the basin, but no low-reflectance signature is seen within the basin (Figures 12a–12f). This observation is consistent with the interior smooth plains having embayed Odin-type deposits, implying that the interior plains are younger.

[26] The interpretation that Odin-type plains are Caloris ejecta is also consistent with stratigraphic relations showing discrete regions of hummocky plains that appear to be embayed by smooth plains exterior to the basin containing more isolated exposures of knobs (Figure 8). These relations may indicate that the hummocky plains once covered a wider area but were buried in part by later volcanic deposits. The isolated knobs within the smooth plains could represent kipukas (preexisting terrain flooded by lavas to produce an island-like exposure) of this underlying hummocky unit, as suggested by *Fassett et al*. [2009].

[27] However, regional crater size–frequency distributions do not support a sequence of events in which Odin-type plains were emplaced as part of the Caloris impact event and are thus the oldest plains associated with the basin. Of the three areas we examined exterior to Caloris, the hummocky plains have the smallest number of superposed craters, implying the youngest age (Table 1, Figure 7). They also show the largest difference from the crater size–frequency distribution measured for Caloris rim materials by *Fassett et al*. [2009]. If the formation of these plains accompanied the formation of the Caloris basin, the plains and basin should have a similar age. The relative crater populations contradict the observed stratigraphic relationships.

[28] How can this conflicting evidence be reconciled? One possible explanation is that the observed differences in the crater populations (Table 1) are not statistically significant and the units are similar in age. Such a statement clearly holds for differences among the Caloris plains, given the overlap in uncertainties. However, this explanation does not address the larger difference in crater size–frequency distribution between hummocky plains and Caloris rim materials [*Fassett et al*., 2009], which is more difficult to attribute to overlapping uncertainties, particularly at the larger crater diameters. Moreover, the Caloris rim size–frequency distribution displays the characteristic Population 1 shape of the late heavy bombardment [*Fassett et al*., 2009, 2011], but that for the hummocky plains does not. If hummocky plains are Caloris ejecta, they should share this trait. Perhaps some physical characteristic of the ejected

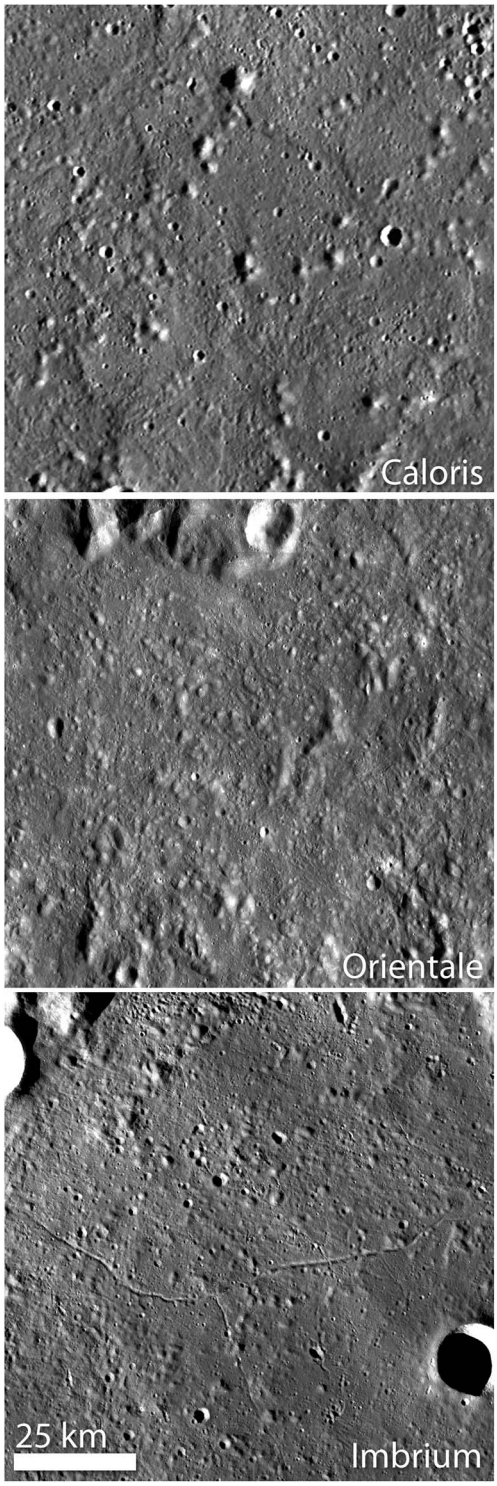

Figure 11. A comparison of knobby terrain associated with the Caloris basin on Mercury (32.5°N, 197.3°E) and with the Orientale (6.9°S, 265.1°E) and Imbrium (65.7°N, 4.1°E) basins on the Moon. Lunar examples are from a Lunar Reconnaissance Orbiter Camera base map with a pixel scale of 100 m. The scale bar applies to all panels.

material (e.g., physical strength of the material) resulted in smaller crater sizes for a given projectile size [*Schultz et al*., 1977; *van der Bogert et al*., 2010; *Hiesinger et al*., 2012]. Another possibility is that the crater population of the Caloris rim was substantially affected by the fallback of Caloris ejecta, such that some significant portion of the craters observed are secondaries from the Caloris event itself that did not affect fluidized ejecta and impact melt emplaced in a different manner at a slightly later time and greater distance. For smaller craters, impact melt has been shown to be emplaced late in the crater excavation stage after the majority of fragmental ejecta [e.g., *Howard and Wilshire*, 1975; *Hawke and Head*, 1977; *Denevi et al*., 2012], suggesting that any fluidized material from the Caloris basin may have been deposited immediately after the majority of near-field secondary cratering. If the crater size–frequency distributions are representative of real age differences, however, then all of the circum-Caloris plains have been resurfaced, no large exposures of Caloris ejecta remain, and some other process is responsible for the hummocky texture observed in Figures 7d, 8, and 12.

[29] Another important aspect of the circum-Caloris plains, including both the Odin-type plains and the majority of the circum-Caloris smooth plains, is their low reflectance and shallow spectral slope, spectral characteristics more similar to those of low-reflectance material (LRM) typically concentrated in basin ejecta, such as that surrounding the Tolstoj basin [*Rava and Hapke*, 1987; *Robinson et al*., 2008; *Denevi et al*., 2009]. The circum-Caloris plains are only ~15% lower in reflectance than the global average, compared with up to 30% lower for LRM, but the diffuse color boundaries between interfingered low-reflectance plains and nearby higher-reflectance plains and the lack of clear color or stratigraphic contacts with the Caloris rim do not support a volcanic interpretation. The most straightforward explanation is that the color properties are consistent with a mixture of materials ejected from depth and deposited around the basin. An alternative hypothesis for the compositional contrast between the exterior and interior plains is that the Caloris impact caused regional changes in mantle dynamics, leading to different depths of partial melting to produce the magmas that formed the different plains [*Roberts and Barnouin*, 2012].

[30] The circum-Caloris plains are not the only low-reflectance smooth plains. Another example is found near 15°N, 47°E, a region far from any large basins, unlikely to have been emplaced as ejecta, and thus interpreted here to be volcanic in origin. A large region of low-reflectance smooth plains is also found ~350 km north of Beethoven basin and another ~150 km northwest of Rembrandt basin, but the proximity of these two areas to these large basins leaves open the possibility that the plains are of impact origin. An irregular, rimless depression that we interpret to be volcanic in origin is found within a region of low-reflectance plains to the northwest of Caloris (Figure 13). Although not all volcanic vents are sources of effusive volcanism on Mercury [e.g., *Head et al*., 2011], they are often found proximal to effusive volcanic deposits, so this feature lends credence to a volcanic origin for at least some LBP units.

[31] Altogether, we find that for ~65% of the smooth plains mapped here, there are multiple lines of evidence for a volcanic origin (e.g., flooding and embayment relationships, color contrasts with surrounding terrain, relationship with volcanic vents). This fraction encompasses all areally extensive units apart from the circum-Caloris plains, of

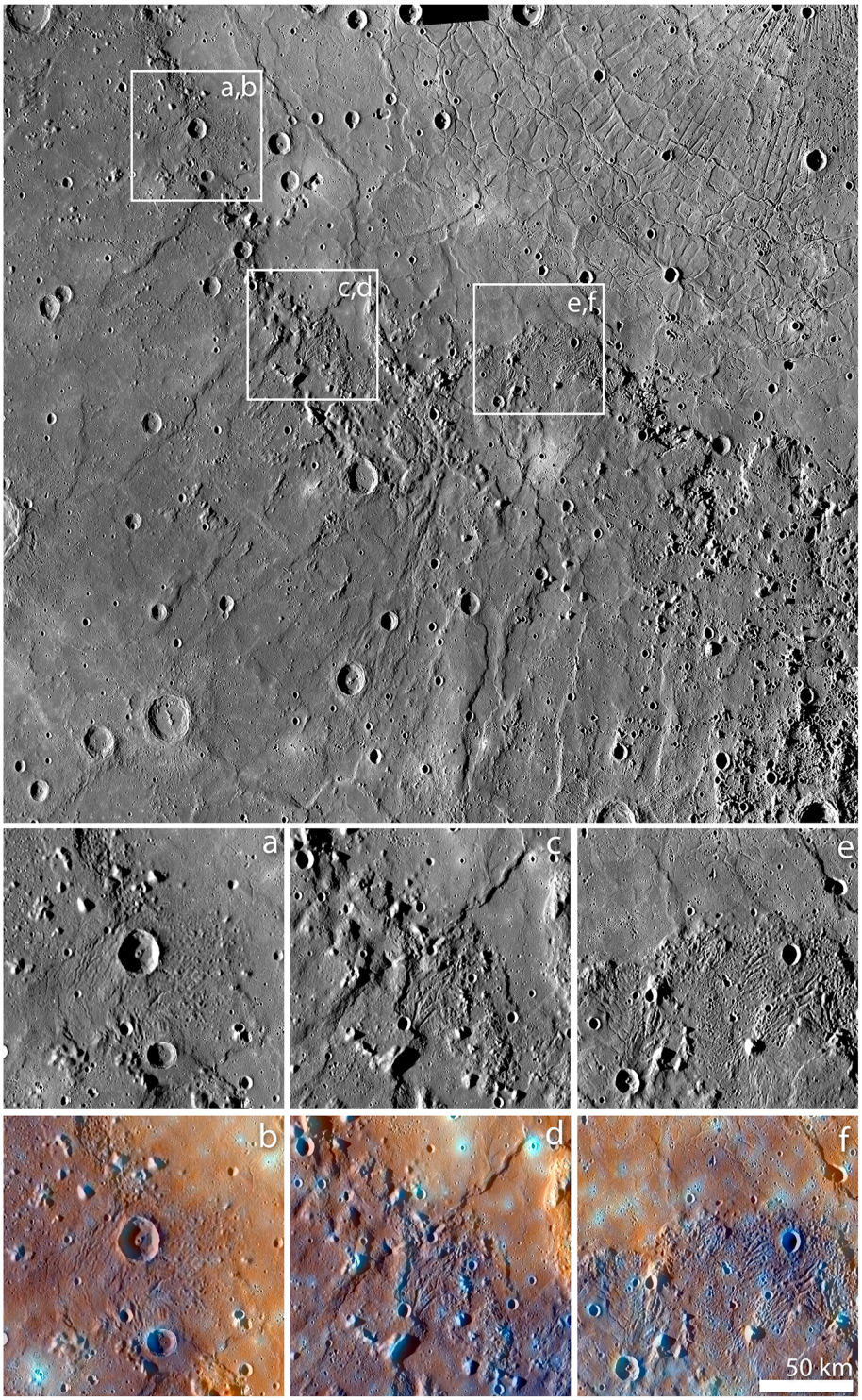

Figure 12. The southwestern portion of the Caloris basin. In the context image (top), knobby plains are observed to grade smoothly to the Caloris rim. (a–f) Three regions at the rim where evidence for channelized flow from the Odin-type plains into the basin is observed. Each region is shown from the monochrome base map (a, c, e) and in enhanced color (b, d, f); the second principal component, first principal component, and 430/1020 nm ratio are shown in red, green, and blue, respectively. A sharp color contrast is observed between the spectrally distinct interior plains and rim deposits, implying that the interior plains superpose material that flowed into the basin. The scale bar in (f) applies as well to (a–e).

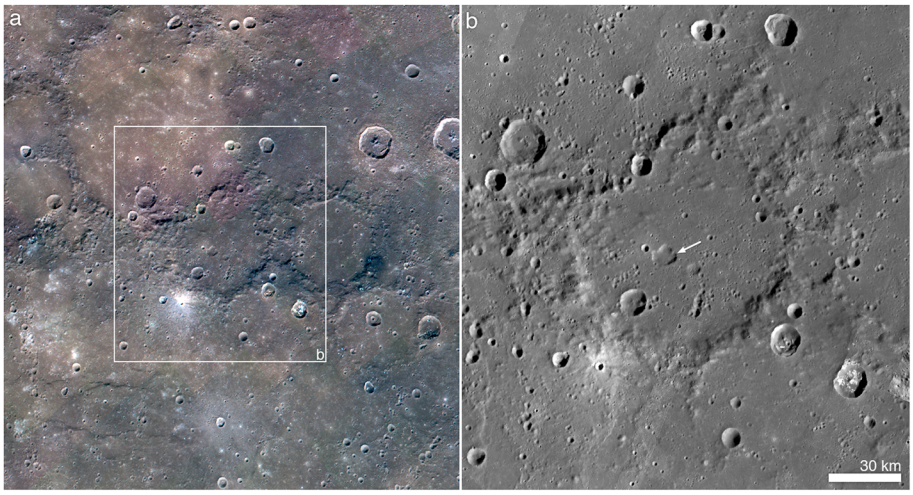

Figure 13. (a) A color image of a region of LBP northwest of Caloris basin (20°N, 50°E). Images from the WAC filters centered on 1000, 750, and 430 nm wavelength are displayed in red, green, and blue, respectively. The location of Figure 13b is indicated. (b) A higher-resolution monochrome view of a possible volcanic vent within this area of LBP, supporting a volcanic origin for at least some LBP.

which only the portions to the south and east with the strongest evidence for volcanism are included in this count. Most of the uncertainty in the remaining fraction lies in the smaller patches that often lack color contrasts with their surroundings and in deposits contained entirely within a crater or basin that may have formed from impact melt, such as in Raditladi.

[32] Although we find strong evidence in support of a volcanic origin for the majority of smooth plains deposits, finding definitive evidence in favor of an origin as fluidized ejecta for some fraction of the plains is difficult. For lunar light plains, the primary evidence from imaging for a different origin from that of the mare deposits is their high albedo, which is not a useful discriminator for Mercury. Many examples of smooth plains deposits clustered within topographic lows around basins, such as Beethoven, have distributions consistent with ejecta emplacement, but these units typically have spectral properties that indicate a compositional difference from adjacent terrain, or they embay craters superposed on the basin, characteristics that favor a volcanic origin. We find several regions where smooth plains without distinct color properties embay rough terrain covered in secondary craters (Figure 14). One area where an impact origin for smooth plains is strongly supported is at Kuiper crater, where ejecta or melt ponded outside the crater, covering secondaries from the Kuiper impact (Figure 14a) [*Beach et al.*, 2012; *D'Incecco et al.*, 2012]. It is likely that some other deposits with similar morphology (e.g., Figure 14b) also formed from impact events. However, many of the regions containing such deposits are located farther from likely source craters or basins than the examples in Figure 14.

4.2. Ages

[33] Crater size–frequency distributions can be used to estimate the absolute ages of a surface given a model for the production of craters on a body. In the case of Mercury,

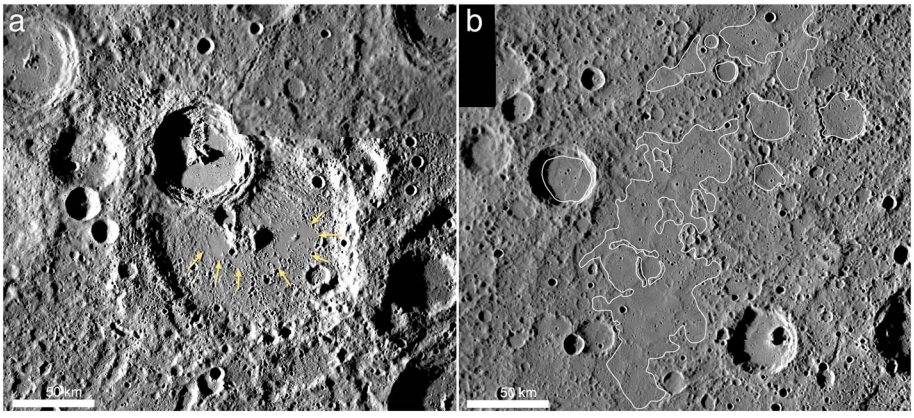

Figure 14. (a) Ejecta and impact melt (yellow arrows) from Kuiper crater embay a field of secondary craters created by the impact event (15°S, 330°E). These characteristics might provide an explanation for other regions where smooth plains deposits are patchy and appear to partially bury a region with a large population of secondary craters, such as that seen in Figure 14b. (b) A region of smooth plains (outlined in white) could be impact melt from Rajnis crater (~80 km in diameter), which is just outside the frame to the east, ~40 km from the edge of the deposit (5°N, 260°E).

many unknowns remain in estimating absolute age from crater density, and thus in the preceding sections we presented our results in terms of $N(20)$ values, which are not model dependent and can be easily compared. However, as a first look at absolute ages we applied the crater chronology model of *Strom and Neukum* [1988] by fitting an isochron to craters larger than 10 km in diameter. From this model, the representative large-scale smooth plains units in Table 1 all have estimated ages between ~3.7 and 3.9 Ga. These estimates are consistent with previous results for the Caloris interior plains [*Strom et al*., 2008, 2011; *Fassett et al*., 2009] and for the northern plains [*Head et al*., 2011; *Ostrach et al*., 2011], which also have estimated ages of ~3.7–3.8 Ga. Although small patches of smooth plains may have ages that extend into the Mansurian with ages as young as 1 Ga [*Prockter et al*., 2010], we find no large expanses with young ages that would be comparable to the lunar Oceanus Procellarum, which includes plains with ages estimated to be 1–2 Ga [*Hiesinger et al*., 2003]. Thus, all major smooth plains units dated thus far, accounting for ~60% of the mapped plains, may have formed within ~200 My, a relatively short interval in Mercury's geologic history. If this result holds in spite of the much larger size and implied longer planetary cooling time of Mercury than of the Moon, the difference in duration of plains volcanism may indicate that the compressional stress state of Mercury's lithosphere [e.g., *Strom et al*., 1975; *Solomon et al*., 2008; *Wilson and Head*, 2008; *Watters et al*., 2009b] worked to inhibit voluminous volcanic eruptions later in Mercury's history [e.g., *Solomon*, 1978; *Chapman*, 1988]. However, the determination of absolute ages can vary substantially (on the order of 1 Gy) with the cratering chronology model used for Mercury [*Ostrach et al*., 2011]. Further work on the determination of ages of surface units would help in understanding the timing of smooth plains emplacement on Mercury.

4.3. Crustal Asymmetry

[34] As noted above, the distribution of smooth plains across Mercury is not uniform. A marked lack of plains is observed south of ~45°S and near 0°E (Figures 1 and 9). What is the cause of this global asymmetry? One hypothesis for the nearside–farside asymmetry in smooth plains (maria) on the Moon is that it resulted from hemispherical differences in mantle temperature, due in part to differences in radioactive element abundances in the uppermost mantle that resulted in generally cooler temperatures in the farside mantle and less production of basaltic partial melt [e.g., *Wieczorek and Phillips*, 2000; *Wieczorek et al*., 2001]. Spatial variations in radioactive elements, if they mirror similar variations at mantle depths, could indicate a tendency for increased melting and volcanism in some regions later in Mercury's history, but no evident correlation between young plains and radioactive element concentrations is observed in Mercury's northern hemisphere [*Peplowski et al*., 2012]. However, diurnal heating of the surface may have resulted in the mobilization and redistribution of K [*Peplowski et al*., 2012], which may have obscured any such relationship. Moreover, radioactive element abundance information is not available for the southern hemisphere. Any spatial relationship between radioactive element abundances and volcanic plains may thus not be resolvable at this time.

[35] On the Moon, regional variations in the thickness of the upper highlands crust, lower in density than mare basalt magma [*Wieczorek et al*., 2013], also likely played a role in determining the locations of eruptions, as a thinner crust increases the likelihood that basaltic magma can ascend to the surface [e.g., *Solomon*, 1975; *Head and Wilson*, 1992; *Shearer et al*., 2006; *Whitten et al*., 2011]. In Mercury's northern hemisphere, some smooth plains units are in areas of lower than average crustal thickness [*Smith et al*., 2012], but there is no general correlation between smooth plains locations and relatively thin crust (Figure 10); the lack of estimates for crustal thickness in the southern hemisphere prevents a global assessment of this relationship. Moreover, surface elemental compositions on Mercury lie within a narrower range than on the Moon, with elemental ratios consistent with magnesian basalt-like to more ultramafic lithologies [*Nittler et al*., 2011; *Weider et al*., 2012]. This narrower range suggests that magmas on Mercury may generally have densities similar to or lower than the densities of crustal rocks, reducing the likelihood that a low-density crust inhibited eruptions to the surface in regions of increased thickness. The observed compositional variations are also consistent with a range of volcanic surface materials formed through different degrees of partial melting [*Weider et al*., 2012]. Previous geologic interpretations of the intercrater plains [*Malin*, 1976; *Strom*, 1977; *Spudis and Guest*, 1988] suggest that much of the surface may be volcanic. Thus, we suggest that Mercury's asymmetry of smooth plains distribution may reflect a different age of the most recent large-scale volcanism rather than a difference in crustal formational processes. Future work assessing the distribution and origin of intercrater plains will be essential to an evaluation of this suggestion.

5. Conclusions

[36] Mercury's surface is covered by ~27% smooth plains, and Odin-type knobby plains comprise an additional 2% of the surface. The crater size–frequency distributions of these plains suggest emplacement after the majority of the late heavy bombardment and possibly within a relatively narrow range of time for the largest expanses of plains. The majority (at least 65%) of these plains are volcanic in nature, with clear flooding and embayment relationships and color and compositional contrasts with underlying terrain.

[37] We find conflicting evidence as to the question of the origin of the circum-Caloris plains. Regions mapped as Odin-type plains share strong morphologic similarities with lunar basin deposits, and they often grade smoothly to the Caloris rim. Both the Odin-type plains and the majority of the circum-Caloris smooth plains share a relatively low reflectance and shallow spectral slope and display no color contrasts with rim deposits. Stratigraphic relationships suggest that Odin-type plains were embayed by local smooth plains that may have been effusively emplaced, and that the isolated knobs within smooth plains may be kipukas of the hummocky unit. Alternatively, both units may be facies of the Caloris basin ejecta. However, the hummocky plains to the east of Caloris have slightly lower crater densities than other plains associated with Caloris, and all circum-Caloris plains are less cratered than the Caloris rim, suggesting they could not have formed contemporaneously with the basin.

Thus, if any of the circum-Caloris plains are material ejected by the Caloris impact event, the crater size–frequency distributions in these regions are not meaningful discriminators of age. The conflicting scenarios presented by the morphologic, stratigraphic, and color relationships, on one hand, and the crater size–frequency distributions, on the other, could be reconciled if either physical properties of the hummocky plains led to differences in crater sizes for given impactor dimensions, or some process, such as near-field secondary cratering, resulted in a higher population of craters on the Caloris basin rim than on the hummocky ejecta. If the crater populations are representative of age, then neither the smooth plains around Caloris nor the Odin-type plains are Caloris ejecta, and some other process is responsible for the characteristic texture of the hummocky plains.

[38] The majority of the smooth plains are relatively high in reflectance, consistent with low-iron basalt-like compositions by inference from XRS elemental compositions of the northern and Caloris interior plains [*Nittler et al*., 2011; *Weider et al*., 2012]. Several regions of smooth plains with low reflectance and relatively shallow spectral slopes (e.g., the plains near 15°N, 47°E; plains north of Beethoven; and plains northwest of Rembrandt) may correspond to more mafic lithologies, indicating that high temperatures and greater degrees of partial melting were possible in mantle source regions relatively late in Mercury's history. If of volcanic rather than impact origin, the circum-Caloris smooth plains would more than double the area of more ultramafic plains emplaced subsequent to the end of late heavy bombardment.

[39] Although smooth plains are generally globally distributed, they are more heavily concentrated in northern latitudes and in the hemisphere surrounding Caloris. The uneven distribution of smooth plains may be due to differences in age and thus preservation, rather than formational processes, of surficial material. Much of the older terrain on Mercury may prove to share a volcanic origin with the smooth plains.

[40] **Acknowledgments.** We thank Aileen Yingst and an anonymous reviewer for constructive reviews. This research has made use of the Integrated Software for Imagers and Spectometers (ISIS) of the U.S. Geological Survey. The MESSENGER project is supported by the NASA Discovery Program under contracts NAS5-97271 to The Johns Hopkins University Applied Physics Laboratory and NASW-00002 to the Carnegie Institution of Washington.

References

Beach, M. J., J. W. Head, L. R. Ostrach, M. S. Robinson, B. W. Denevi, and S. C. Solomon (2012), The influence of pre-existing topography on the distribution of impact melt on Mercury, *Lunar Planet. Sci.*, *43*, abstract 1335.

Becker, K. J., L. A. Weller, K. L. Edmundson, T. L. Becker, M. S. Robinson, A. C. Enns, and S. C. Solomon (2012), Global controlled mosaic of Mercury from MESSENGER orbital images, *Lunar Planet. Sci.*, *43*, abstract 2654.

Blewett, D. T., et al. (2011), Hollows on Mercury: MESSENGER evidence for geologically recent volatile-related activity, *Science*, *333*, 1856–1859, doi:10.1126/science.121681.

Boyce, J. M., A. L. Dial, and L. A. Soderblom (1974), Ages of the lunar near side light plains and maria, *Proc. Lunar Sci. Conf*., *5th*, 11–23.

Chapman, C. R. (1988), Mercury: Introduction to an end-member planet, in *Mercury*, edited by F. Vilas, C. R. Chapman, and M. S. Matthews, pp. 1–23, University of Arizona Press, Tucson, Ariz.

Charlier, B., T. L. Grove, and M. T. Zuber (2013), Phase equilibria of ultramafic compositions on Mercury and the origin of the compositional dichotomy, *Earth Planet. Sci. Lett.*, *363*, 50–60.

Crater Analysis Techniques Working Group (1979), Standard techniques for presentation and analysis of crater size-frequency data, *Icarus*, *37*, 467–474.

Denevi, B. W., and M. S. Robinson (2008), Merury's albedo from Mariner 10: Implications for the presence of ferrous iron, *Icarus*, *197*, 239–246, doi:10.1016/j.icarus.2008.04.021.

Denevi, B. W., et al. (2009), The evolution of Mercury's crust: A global perspective from MESSENGER, *Science*, *324*, 613–618.

Denevi, B. W., et al. (2012), Physical constraints on impact melt properties from Lunar Reconnaissance Orbiter Camera images, *Icarus*, *219*, 665–675, doi:10.1016/j.icarus.2012.03.020.

D'Incecco, P., J. Helbert, J. W. Head, M. D'Amore, A. Maturilli, N. R. Izenberg, G. M. Holsclaw, D. L. Domingue, W. E. McClintock, and S. C. Solomon (2012), Kuiper crater on Mercury – An opportunity to study recent surface weathering trends with MESSENGER, *Lunar Planet. Sci.*, *43*, abstract 1815.

Eggleton, R. E., and G. G. Schaber (1972), Cayley Formation interpreted as basin ejecta, in *Apollo 16 Preliminary Science Report*, pp. 29-7–29-16, Special Publication SP-315, NASA, Washington, D.C.

Fassett, C. I., J. W. Head, D. T. Blewett, C. R. Chapman, J. L. Dickson, S. L. Murchie, S. C. Solomon, and T. R. Watters (2009), Caloris impact basin: Exterior geomorphology, stratigraphy, morphometry, radial sculpture, and smooth plains deposits, *Earth Planet. Sci. Lett.*, *285*, 297–308.

Fassett, C. I., S. J. Kadish, J. W. Head, S. C. Solomon, and R. G. Strom (2011), The global population of large craters on Mercury and comparisons with the Moon, *Geophys. Res. Lett.*, *38*, L10202, doi:10.1029/2011GL047294.

Gaskell, R. W., E. E. Palmer, N. Mastrodemos, O. S. Barnouin, L. Jorda, and A. H. Taylor (2011), Mercury and Vesta - Preliminary shape and topography, abstract P41A–1576, presented at 2011 Fall Meeting, American Geophysical Union, San Francisco, Calif., 5–9 December.

Gillis-Davis, J. J., D. T. Blewett, R. W. Gaskell, B. W. Denevi, M. S. Robinson, R. G. Strom, S. C. Solomon, and A. L. Sprague (2009), Pit-floor craters on Mercury: Evidence of near-surface igneous activity, *Earth Planet. Sci. Lett.*, *285*, 243–250, doi:10.1016/j.epsl.2009.05.023.

Goudge, T. A., et al. (2012), Global inventory and characterization of pyroclastic deposits on Mercury: New insights into pyroclastic activity from MESSENGER orbital data, *Lunar Planet. Sci.*, *43*, abstract 1325.

Grolier, M. J., and J. M. Boyce (1984), Geologic map of the Borealis region of Mercury, Map I-1660, Misc. Investigations Ser., U. S. Geological Survey, Denver, Colo.

Guest, J. E., and R. Greeley (1983), Geologic map of the Shakespeare quadrangle of Mercury, Map I-1408, Misc. Investigations Ser., U. S. Geological Survey, Denver, Colo.

Hapke, B., C. Christman, B. Rava, and J. Mosher (1980), A color-ratio map of Mercury, *Proc. Lunar Planet. Sci. Conf*., *11th*, 817–821.

Hawke, B. R., and J. W. Head (1977), Impact melt on lunar crater rims, in *Impact and Explosion Cratering: Planetary and Terrestrial Implications*, edited by D. J. Roddy, R. O. Pepin, and R. B. Merrill, pp. 815–841, Pergamon Press, New York.

Hawkins, S. E., III, et al. (2007), The Mercury Dual Imaging System on the MESSENGER spacecraft, *Space Sci. Rev.*, *131*, 247–338.

Head, J. W., and L. Wilson (1992), Lunar mare volcanism: Stratigraphy, eruption conditions, and the evolution of secondary crusts, *Geochim. Cosmochim. Acta*, *56*, 2155–2175.

Head, J. W., et al. (2008), Volcanism on Mercury: Evidence from the first MESSENGER flyby, *Science*, *321*, 69–72.

Head, J. W., et al. (2009a), Volcanism on Mercury: Evidence from the first MESSENGER flyby for extrusive and explosive activity and the volcanic origin of plains, *Earth Planet. Sci. Lett.*, *285*, 227–242, doi:10.1016/j.epsl.2009.03.007.

Head, J. W., et al. (2009b), Evidence for intrusive activity on Mercury from the first MESSENGER flyby, *Earth Planet. Sci. Lett.*, *285*, 251–262, doi:10.1016/j.epsl.2009.03.008.

Head, J. W., et al. (2011), Flood volcanism in the northern high latitudes of Mercury revealed by MESSENGER, *Science*, *333*, 1853–1856.

Hiesinger, H., J. W. Head, U. Wolf, R. Jaumann, and G. Neukum (2003), Ages and stratigraphy of mare basalts in Oceanus Procellarum, Mare Nubium, Mare Cognitum, and Mare Insularum, *J. Geophys. Res.*, *108*(E7), 5065, doi:10.1029/2002JE001985.

Hiesinger, H., C. H. van der Bogert, J. H. Pasckert, L. Funcke, L. Giacomini, L. R. Ostrach, and M. S. Robinson (2012), How old are young lunar craters?, *J. Geophys. Res.*, *117*, E00H10, doi:10.1029/2011JE003935.

Howard, K. A., and H. G. Wilshire (1975), Flows of impact melt at lunar craters, *J. Res. U. S. Geol. Survey*, *3*, 237–251.

Kerber, L., J. W. Head, S. C. Solomon, S. L. Murchie, D. T. Blewett, and L. Wilson (2009), Explosive volcanic eruptions on Mercury: Eruption conditions, magma volatile content, and implications for interior volatile abundances, *Earth Planet. Sci. Lett.*, *285*, 263–271, doi:10.1016/j.epsl.2009.04.037.

Kerber, L., J. W. Head, D. T. Blewett, S. C. Solomon, L. Wilson, S. L. Murchie, M. S. Robinson, B. W. Denevi, and D. L. Domingue (2011), The global distribution of pyroclastic deposits on Mercury: The view from MESSENGER flybys 1–3, *Planet. Space Sci.*, *59*, 1895–1909, doi:10.1016/j.pss.2011.03.020.

King, J. S., and D. H. Scott (1990), Geologic map of the Beethoven quadrangle of Mercury, Map I-2048, Misc. Investigations Ser., U. S. Geological Survey, Denver, Colo.

Klimczak, C., T. R. Watters, C. M. Ernst, A. M. Freed, P. K. Byrne, S. C. Solomon, D. M. Blair, and J. W. Head (2012), Deformation associated with ghost craters and basins in volcanic smooth plains on Mercury: Strain analysis and implications for plains evolution, *J. Geophys. Res.*, *117*, E00L03, doi:10.1029/2012JE004100.

Malin, M. C. (1976), Observations of intercrater plains on Mercury, *Geophys. Res. Lett.*, *3*, 581–584.

McCauley, J. F., J. E. Guest, G. G. Schaber, N. J. Trask, and R. Greeley (1981), Stratigraphy of the Caloris basin, Mercury, *Icarus*, *47*, 184–202.

Murchie, S. L. et al. (2008), Geology of the Caloris Basin, Mercury: A new view from MESSENGER, *Science*, *321*, 73–76.

Murray, B. C., M. J. S. Belton, G. E. Danielson, M. E. Davies, D. E. Gault, B. Hapke, B. O'Leary, R. G. Strom, V. Suomi, and N. Trask (1974), Mercury's surface: Preliminary description and interpretation from Mariner 10 pictures, *Science*, *185*, 169–179.

Murray, B. C., R. G. Strom, N. J. Trask, and D. E. Gault (1975), Surface history of Mercury: Implications for terrestrial planets, *J. Geophys. Res.*, *80*, 2508–2514.

Neukum, G. (1977), Different ages of lunar light plains, *Moon*, *17*, 383–393.

Nittler, L. R., et al. (2011), The major-element composition of Mercury's surface from MESSENGER X-ray spectrometry, *Science*, *333*, 1847–1850.

Oberst, J., F. Preusker, R. J. Phillips, T. R. Watters, J. W. Head, M. T. Zuber, and S. C. Solomon (2010), The morphology of Mercury's Caloris basin as seen in MESSENGER stereo topographic models, *Icarus*, *209*, 230–238, doi:10.1016/j.icarus.2010.03.009.

Ostrach, L. R., C. R. Chapman, C. I. Fassett, J. W. Head, W. J. Merline, M. S. Robinson, S. C. Solomon, R. G. Strom, and Z. Xiao (2011), Crater statistics for the northern polar region of Mercury derived from *MESSENGER* orbital data, *Abstracts with Programs*, *43*(5), paper 142–14, p. 360, Geological Society of America, Boulder, Colo. (CD-ROM).

Peplowski, P. N., et al. (2012), Variations in the abundances of potassium and thorium on the surface of Mercury: Results from the MESSENGER Gamma-Ray Spectrometer, *J. Geophys. Res.*, *117*, E00L04, doi:10.1029/2012JE004141.

Preusker, F., J. Oberst, J. W. Head, T. R. Watters, M. S. Robinson, M. T. Zuber, and S. C. Solomon (2011), Stereo topographic models of Mercury after three MESSENGER flybys, *Planet. Space Sci.*, *59*, 1910–1917.

Preusker, F., J. Oberst, D. T. Blewett, K. Gwinner, J. W. Head, S. L. Murchie, M. S. Robinson, T. R. Watters, M. T. Zuber, and S. C. Solomon (2012), Topography of Mercury from stereo images: First samples from MESSENGER orbital mapping, *Lunar Planet. Sci.*, *43*, abstract 1913.

Prockter, L. M., et al. (2010), Evidence for young volcanism on Mercury from the third MESSENGER flyby, *Science*, *329*, 668–671.

Rava, B., and B. Hapke (1987), An analysis of the Mariner 10 color ratio map of Mercury, *Icarus*, *71*, 397–429.

Roberts, J. H., and O. S. Barnouin (2012), The effect of the Caloris impact on the mantle dynamics and volcanism of Mercury, *J. Geophys. Res.*, *117*, E02007, doi:10.1029/2011JE003876.

Robinson, M. S., and P. G. Lucey (1997), Recalibrated Mariner 10 color mosaics: Implications for mercurian volcanism, *Science*, *275*, 197–200.

Robinson, M. S., et al. (2008), Reflectance and color variations on Mercury: Regolith processes and compositional heterogeneity, *Science*, *321*, 66–69.

Schultz, P. H., R. Greeley, and D. Gault (1977), Interpreting statistics of small lunar craters, *Proc. Lunar Sci. Conf.*, *8th*, 3539–3564.

Shearer, C. K., et al. (2006), Thermal and magmatic evolution of the Moon, in *New Views of the Moon*, *Reviews in Mineralogy and Geochemistry*, *60*, edited by B. L. Jolliff, M. A. Wieczorek, C. K. Shearer, and C. R. Neal, pp. 365–518, The Mineralogical Society of America, Chantilly, Va.

Smith, D. E., et al. (2012), Gravity field and internal structure of Mercury from MESSENGER, *Science*, *336*, 214–217.

Solomon, S. C. (1975), Mare volcanism and lunar crustal structure, *Proc. Lunar Sci. Conf.*, *6th*, 1021–1042.

Solomon, S. C. (1978), On volcanism and thermal tectonics on one-plate planets, *Geophys. Res. Lett.*, *5*, 461–464.

Solomon, S. C., et al. (2008), Return to Mercury: A global perspective on MESSENGER's first Mercury flyby, *Science*, *321*, 59–62.

Spudis, P. D., and J. E. Guest (1988), Stratigraphy and geologic history of Mercury, in *Mercury*, edited by F. Vilas, C. R. Chapman, and M. S. Matthews, pp. 118–164, University of Arizona Press, Tucson, Ariz.

Spudis, P. D., and J. G. Prosser (1984), Geologic map of the Michelangelo quadrangle of Mercury, Map I-1659, Misc. Investigations Ser., U. S. Geological Survey, Denver, Colo.

Stockstill-Cahill, K. R., T. J. McCoy, L. R. Nittler, S. Z. Weider, and S. A. Hauck (2012), Magnesium-rich crustal compositions on Mercury: Implications for magmatism from petrologic modeling, *J. Geophys. Res.*, *117*, E00L15, doi:10.1029/2012JE004140.

Strom, R. G. (1977), Origin and relative age of lunar and mercurian intercrater plains, *Phys. Earth Planet. Inter.*, *15*, 156–172.

Strom, R. G., and G. Neukum (1988), The cratering record on Mercury and the origin of impacting objects, in *Mercury*, edited by F. Vilas, C. R. Chapman, and M. S. Matthews, pp. 336–373, University of Arizona Press, Tucson, Ariz.

Strom, R. G., N. J. Trask, and J. E. Guest (1975), Tectonism and volcanism on Mercury, *J. Geophys. Res.*, *80*, 2478–2507.

Strom, R. G., R. Malhotra, T. Ito, F. Yoshida, and D. A. Kring (2005), The origin of planetary impactors in the inner solar system, *Science*, *309*, 1847–1850.

Strom, R. G., C. R. Chapman, W. J. Merline, S. C. Solomon, and J. W. Head (2008), Mercury cratering record viewed from MESSENGER's first flyby, *Science*, *321*, 79–81.

Strom, R. G., M. E. Banks, C. R. Chapman, C. I. Fassett, J. A. Forde, J. W. III Head, W. J. Merline, L. M. Prockter, and S. C. Solomon (2011), Mercury crater statistics from MESSENGER flybys: Implications for stratigraphy and resurfacing history, *Planet. Space Sci.*, *59*, 1960–1967, doi:10.1016/j.pss.2011.03.018.

Trask, N. J., and D. Dzurisin (1984), Geologic map of the Discovery quadrangle of Mercury, Map I-1658, Misc. Investigations Ser., U. S. Geological Survey, Denver, Colo.

Trask, N. J., and J. E. Guest (1975), Preliminary geologic terrain map of Mercury, *J. Geophys. Res.*, *80*, 2461–2477.

Trask, N. J., and R. G. Strom (1976), Additional evidence of mercurian volcanism, *Icarus*, *28*, 556–563.

van der Bogert, C. H., et al. (2010), Discrepancies between crater size-frequency distributions on ejecta and impact melt pools at lunar craters: An effect of differing target properties?, *Lunar Planet. Sci.*, *41*, abstract 2165.

Watters, T. R. (1988), Wrinkle ridge assemblages on the terrestrial planets, *J. Geophys. Res.*, *93*, 10,236–10,254.

Watters, T. R., S. C. Solomon, M. S. Robinson, J. W. Head, S. L. André, S. A. Hauck II, and S. L. Murchie (2009a), The tectonics of Mercury: The view after MESSENGER's first flyby, *Earth Planet. Sci. Lett.*, *285*, 283–296, doi:10.1016/j.epsl.2009.01.025.

Watters, T. R., S. L. Murchie, M. S. Robinson, S. C. Solomon, B. W. Denevi, S. L. André, and J. W. Head (2009b), Emplacement and tectonic deformation of smooth plains in the Caloris basin, Mercury, *Earth Planet. Sci. Lett.*, *285*, 309–319, doi:10.1016/j.epsl.2009.03.040.

Weider, S. Z., L. A. Nittler, R. D. Starr, T. J. McCoy, K. R. Stockstill-Cahill, P. K. Byrne, B. W. Denevi, J. W. Head, and S. C. Solomon (2012), Chemical heterogeneity on Mercury's surface revealed by the MESSENGER X-Ray Spectrometer, *J. Geophys. Res.*, *117*, E00L05, doi:10.1029/2012JE004153.

Whitten, J., J. W. Head, M. Staid, C. M. Pieters, J. Mustard, R. Clark, J. Nettles, R. L. Klima, and L. Taylor (2011), Lunar mare deposits associated with the Orientale impact basin: New insights into mineralogy, history, mode of emplacement, and relation to Orientale Basin evolution from Moon Mineralogy Mapper (M3) data from Chandrayaan-1, *J. Geophys. Res.*, *116*, E00G09, doi:10.1029/2010JE003736.

Whitten, J. L., J. W. Head, S. L. Murchie, D. T. Blewett, B. W. Denevi, G. A. Neumann, M. T. Zuber, D. E. Smith, and S. C. Solomon (2012), Intercrater plains on Mercury: Topographic assessment with MESSENGER data, *Lunar Planet. Sci.*, *43*, abstract 1479.

Wieczorek, M. A., and R. J. Phillips (2000), The "Procellarum KREEP Terrane": Implications for mare volcanism and lunar evolution, *J. Geophys. Res.*, *105*, 20,417–20,430, doi:10.1029/1999JE001092.

Wieczorek, M. A., M. T. Zuber, and R. J. Phillips (2001), The role of magma buoyancy on the eruption of lunar basalts, *Earth Planet. Sci. Lett.*, *185*, 71–83.

Wieczorek, M. A., et al. (2013), The crust of the Moon as seen by GRAIL, *Science*, *339*, 671–675.

Wilhelms, D. E. (1976), Mercurian volcanism questioned, *Icarus*, *28*, 551–558.

Wilhelms, D. E. (1987), *The Geologic History of the Moon*, Prof. Paper 1348, U. S. Geological Survey, United States Government Printing Office, Washington, D.C.

Wilson, L., and J. W. Head (2008), Volcanism on Mercury: A new model for the history of magma ascent and eruption, *Geophys. Res. Lett.*, *35*, L23205, doi:10.1029/2008GL035860.

Zuber, M. T., et al. (2012), Topography of the northern hemisphere of Mercury from MESSENGER laser altimetry, *Science*, *336*, 217–220.